

SUPPLEMENTAL MATERIAL FOR MANUSCRIPT: SMALL-SCALE DEMIXING IN  
CONFLUENT BIOLOGICAL TISSUES

Simulation Parameters

Here we provide tables for the parameters used for each aspect of the simulations. For our dynamical simulations, the systems are equilibrated for time,  $t_{eq}$ , and subsequently run for a longer time. For our FIRE simulations, simulations typically run until the maximum force experienced by a vertex reduces below a threshold value of  $10^{-13}$ .

TABLE S1. Shape Bi-disperse Dynamical Simulations TABLE S2. Area Bi-disperse Dynamical Simulations

Parameters	values
1. Ensembles	50
2. $s_{av}$	3.79- 3.91
3. $\Delta$	0.0-0.4
4. $t_{eq}$	1000
5. $dt$	0.001
6. $(K_a, K_p)$	(100,1)
7. $T$	0.01
8. $N$	400
9. Total time	$2 \times 10^5 + t_{eq}$
10. $l_c$	0.04
11. HLT ( $\gamma$ ) for $p_0 = 3.97$	0.1

Parameters	values
1. Ensembles	50
2. $s_0$	3.85
3. $\alpha$	1.0-2.5
4. $t_{eq}$	1000
5. $dt$	0.01
6. $(K_a, K_p)$	(1,1)
7. $T$	0.01
8. $N$	400
9. Total time	$2 \times 10^5 + t_{eq}$
10. $l_c$	0.04
11. $\langle A_0 \rangle$	1

TABLE S3. FIRE minimization for  $E_s/E_m$

Parameters	values
1. Ensembles	250
2. $s_{av}, s_0$	3.85
3. $\alpha$	1.0-2.5
4. $\Delta$	0-0.12
5. $dt$	0.01
6. $K_a$	$1(\alpha)$ & 100 ( $\Delta$ )
7. $T$	0.01
8. $N$	100,400,900
9. Maximum FIRE steps	$10^5$
10. $l_c$	0.04

TABLE S4. T1 energy barriers

Parameters	values
1. Ensembles	250
2. $s_{av}$	3.79-3.88
3. $\alpha$	1.0-2.5
4. $s_0$	3.82-3.88
5. $dt$	0.01
6. $K_a$	$1(\alpha)$ & 100 ( $\Delta$ )
7. $T$	0.01
8. $N$	80
9. Maximum FIRE steps	$10^5$
10. $l_c$	0.04
11. $\Delta$	0-0.12

Effect of area stiffness on fluidity

High shape-disparity can amplify coarsening in mixtures, resulting in further enhanced disparity in cell areas. To prevent this coarsening from occurring, we increase the area stiffness  $K_a$  to 100. To make sure this does not affect the fluid phase seen in monodisperse mixtures, we study the effective diffusivity as a function of the target shape parameter for several  $K_a$  values. We find that  $K_a$  barely affects the diffusivities and that the large changes in curvature of  $D_{eff}$  versus  $s_0$  remain close to 3.81 such that larger values of  $K_a$  do not significantly affect the fluidity of the cells. See Fig. S1.

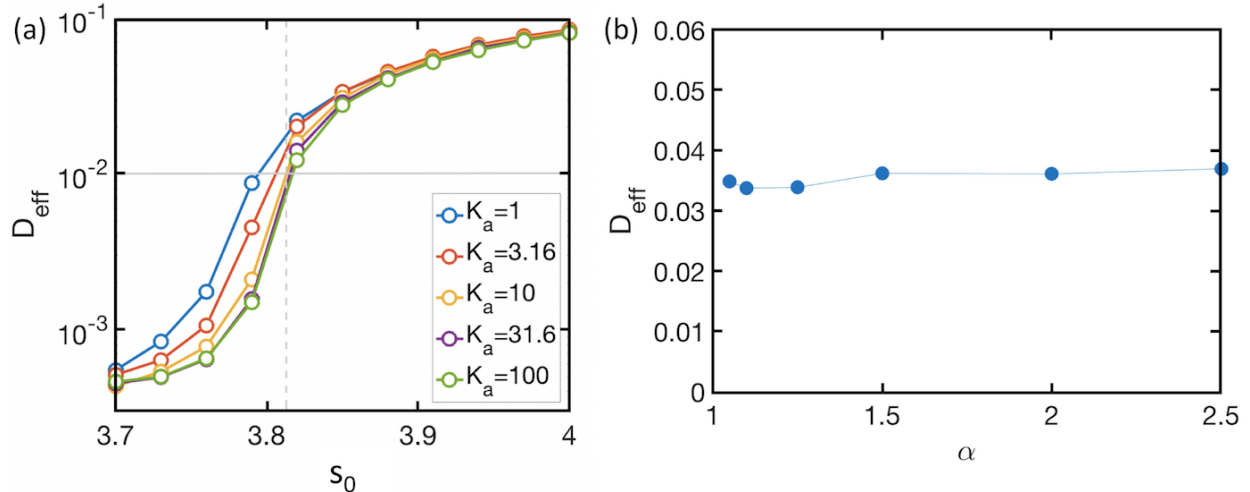


FIG. S1. (a) *Effective diffusivity ( $D_{\text{eff}}$ ) with respect to target shape parameter  $s_0$ .* Different curves are for monodisperse systems with  $K_a$  varying from 1 to 100. The solid horizontal line represents the cutoff at 0.01 used previously. The vertical dashed line denotes  $s_0^* = 3.813$ . (b) *Effective diffusivity in area bidisperse mixtures.* Plot of the effective diffusivity ( $D_{\text{eff}}$ ) with respect to increasing area dispersity  $\alpha$ . Parameter details provided in Table S2.

### Diffusivity of area bidisperse mixtures

Monodisperse systems with  $s_0 > 3.81$  have a fluid-like diffusivity. Here we check diffusivity for mixtures having the same  $s_0 = 3.85$  for all cell types but bidisperse in size. We see that the average fluid-like diffusivity remains unchanged. See Fig. S1b.

### Component-wise diffusivity and timescales in shape bidisperse mixtures

We study the diffusivities of individual components for mixtures with fixed  $s_{av} = 3.85$ . Although increased dispersity signals a solid-fluid mixture, we see that the average behavior remains fluid-like up to high dispersities. Hence, we measure the diffusivity of each component to determine if the solid-like cells diffuse (Fig. S2a). We find that a fluid-like component is indeed able to help the solid-like cells diffuse.

For the demixing observed in shape bidisperse mixtures, as mentioned in the main text, we observe that for most of the  $\Delta$ , the DP saturates to a final value. We check if the timescale associated with this saturation increases with dispersity since Fig. S2a demonstrates that the solid components (of high dispersity mixtures) do not diffuse as much. We define  $t_{1/2}$  as the average time taken by the system to get to half of its final DP. We observe that this half-time increases exponentially with  $\Delta$ , as shown in the inset of Fig. S2b.

### Increasing temperature decreases micro-demixing

Since we hypothesize that micro-demixing is due to kinetic traps between energy barriers to neighbor exchanges, raising the temperature so that cells should be able to surmount such energy barriers should lead to complete mixing. We, therefore, study the micro-demixing as a function of an increased temperature in a mixture with fixed dispersity  $\Delta = 0.2$ . We observe that increasing temperature indeed leads to complete mixing, i.e. the demixing parameter goes to zero. For an

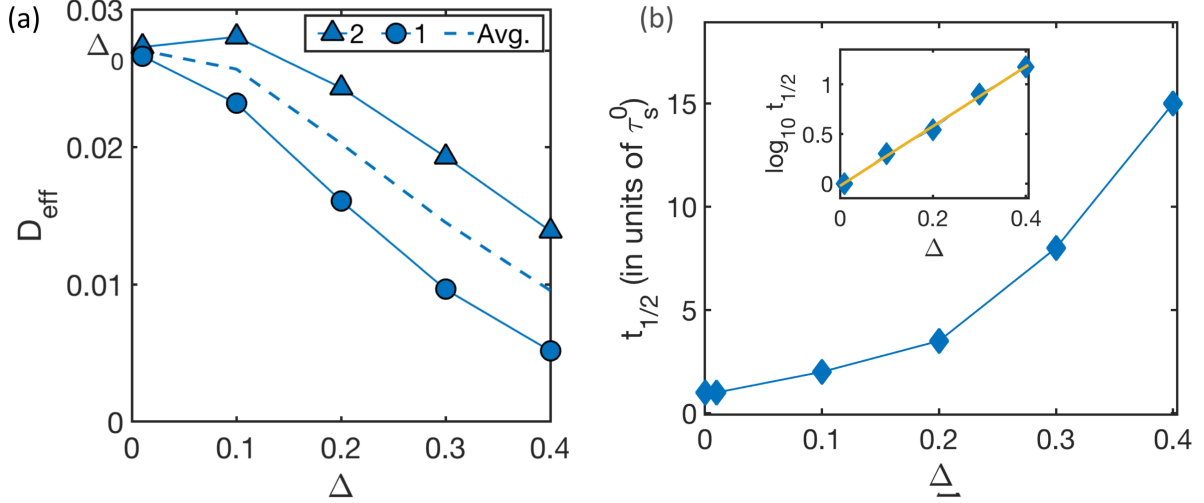


FIG. S2. *Component-wise diffusivities and timescale to approach steady state.* (a) Plot for effective diffusivity ( $D_{eff}$ ) with respect to increasing shape dispersity  $\Delta$ . The solid lines are for the two different components with triangles and circles representing higher  $s_0$  (type 2) and lower  $s_0$  (type 1) respectively. The dashed curve represents the averaged  $D_{eff}$ . (b) The average time it takes for the system to achieve half of its steady state DP value, or  $t_{1/2}$ , is plotted against  $\Delta$ . The solid curves from 2(b) are used to compute  $t_{1/2}$ . The inset shows log-log plot of the same, with a linear fit in solid yellow line is  $y = 3x + 3$ .

increased temperature we use the relation  $\tau_\alpha \propto T^{-3/2}$ , reported in [48], to re-scale the x-axis. The lower temperatures systems have yet to reach a steady state demixing value. One can use a strip geometry to probe the exact steady state value for lower temperatures, which we leave for future work.

### Cortical tension for sorted vs. mixed configurations

An emergent line tension between two different kinds of cells must show a high line tension along heterotypic edges and lower line tension along the homotypic edges. Hence, for both the sorted and mixed scenarios (Fig. 4), we study a *line tension map* where the thickness of the edge is linearly proportional to its line tension. A positive value is colored in red and a negative value is colored in blue. The cortical tension for each edge can be computed using the method suggested in Ref. [38].

The cortical tension analysis conveys the fact that there is no emergent line tension due to bidispersity in the mixtures we study. The mean heterotypic line tension (black vertical line) is less than or equal to the mean homotypic line tension (colored vertical line) for all the scenarios. See Figs. S4 and S5.

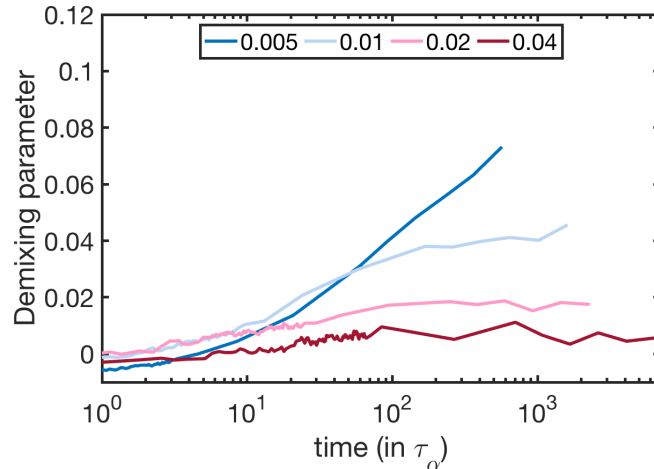


FIG. S3. *Increasing temperature, diminishes observed demixing.* (a) Plot for demixing parameter ( $DP$ ) with respect to time (in units of  $\tau_\alpha$ ). The solid curves represent an increasing temperature ( $T$ ) from blue ( $T = 0.005$ ) to maroon ( $T = 0.04$ ). The curves are averaged over 280 ensembles.

### Differential T1 energy barriers in area bidisperse mixtures

We present data supporting the notion that the differential energy barriers are smaller for the area bidisperse mixtures as compared to the shape bidisperse ones. We focus on larger cells trying to invade a cluster of smaller cells and vice versa to determine the stability (or lack thereof) an interface. See Fig. S6. We also present data for other types of topologies for both shape and area bidisperse mixtures for completeness (see Fig. S9).

Finally, to study differential T1 energy barriers in a simplified setting, we consider four cells connected to each other symmetrically. The energy is minimized with respect to a diminishing T1 edge length  $l$  using MATLAB. The area stiffness is kept very high and the initial condition is recursively fed from a longer  $l$  energy minimized configuration to the subsequent shorter  $l$ . We can accommodate different sizes and shapes as long as cells of different types are positioned symmetrically about both  $x$  and  $y$  axis and make the cells sharing the T1 edge (T1 pair) have different properties from the non-T1 pair. The formula used to compute energy barrier is  $E(l = l_H) - E(l = 0)$ , where  $l_H$  is the edge length of a uniform hexagon with unit area.

To study the effect of shape bidispersity (Fig. S7), the energy barrier (red when non-zero and blue when vanishingly small) is plotted with respect to the shape of T1 pair (x-axis) and the shape of the non-T1 pair (y-axis), which can be independently varied. A similar analysis is done for mixtures with bidisperse areas (Fig. S8). We observe differential energy barriers in both cases with, again, the size of the barrier generically larger in the shape bidisperse case as compared to the area bidisperse case, even in this simplified calculation. Re-phrasing this in terms of invading a cluster of the opposite type, one can think of these as invading doublets of opposite kind.

### Additional experimental features

Figure S10 provides additional information regarding the motility of the cells (Fig. S10a), the distribution of cell areas (Fig. S10b), and the ratio of the numbers of the two cell types during the course of the experiment (Fig. S10c). There is little difference in the amount of the displacement the two different cell types undergo within 24 hours either in the monotypic monolayers or in the

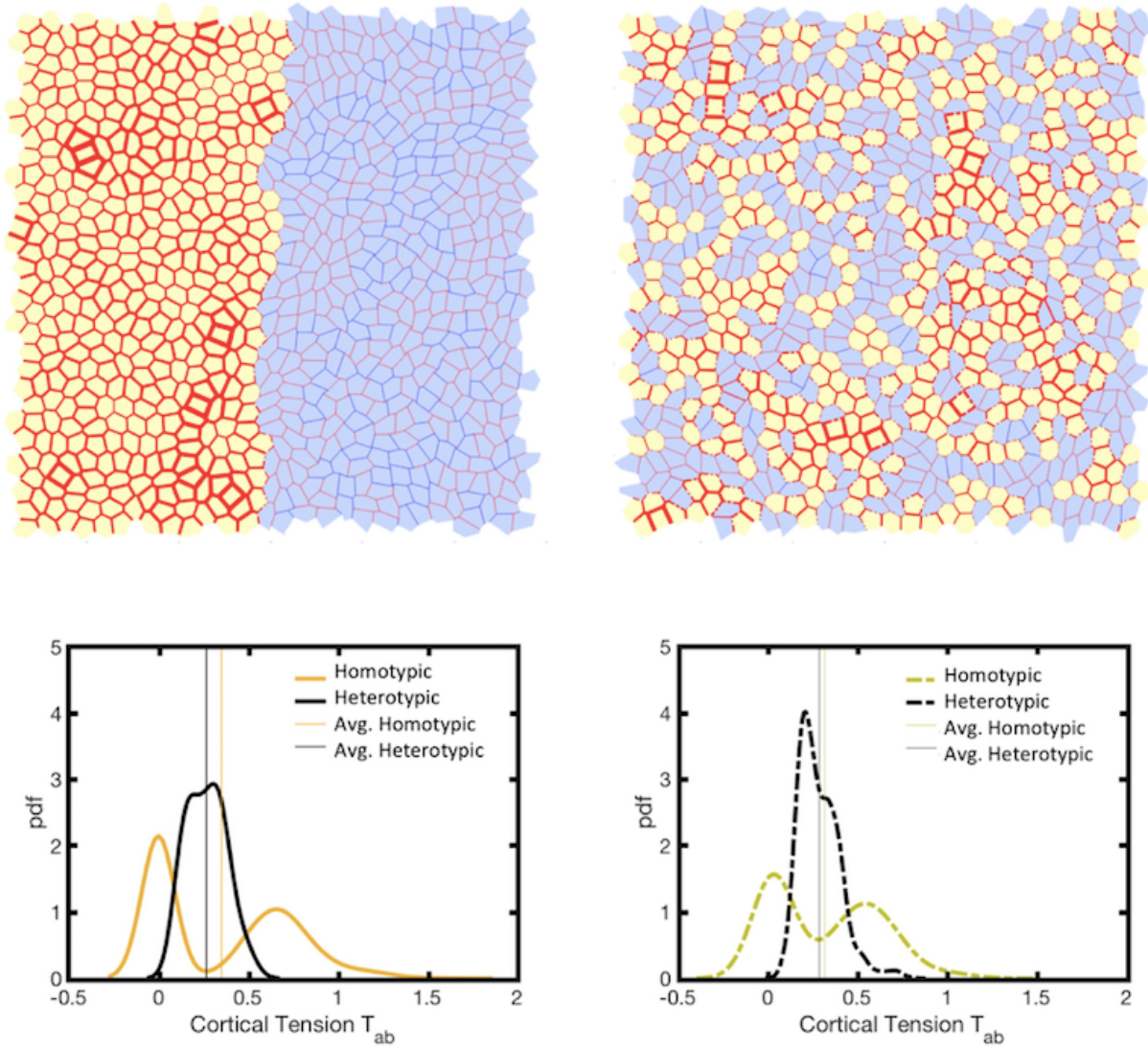


FIG. S4. *Cortical tension in shape bidisperse mixtures of  $\Delta = 0.4$ .* Left and right panels shows line tension maps for sorted and mixed scenarios for a  $N = 900$  system respectively. Heterotypic edges are shown in dash-dot lines. Yellow and blue cells have  $p_0 = 3.65$  and  $4.05$  respectively. They are followed by histograms for heterotypic (in black) and homotypic (colored) edges. Vertical lines show the mean values for each curve in their respective colors.

combined monolayers. There is also minimal difference in the distribution of cell areas for the two different cell types as measured in the respective monotypic monolayer (Fig. S10b). Finally, Fig. S10c demonstrates that the Ctr-E-cad<sup>-/-</sup> mixtures remain approximately 50:50 mixtures over the duration of the experiments.

We verify that natural variability in adhesion from cell-to-cell does not drive micro-demixing by calculating the demixing parameter (DP) for monotypic monolayers with half the cells tagged with one type of stain and the other half tagged with a second stain (Fig. S11a). We find that the demixing parameter does not increase (or decrease) on average with time, strongly suggesting that differential adhesion is indeed what is driving the micro-demixing.

In addition to computing the demixing parameter for the co-culture, we also study the pair correlation functions between all the three possible cell-type pairs in the co-culture in the high

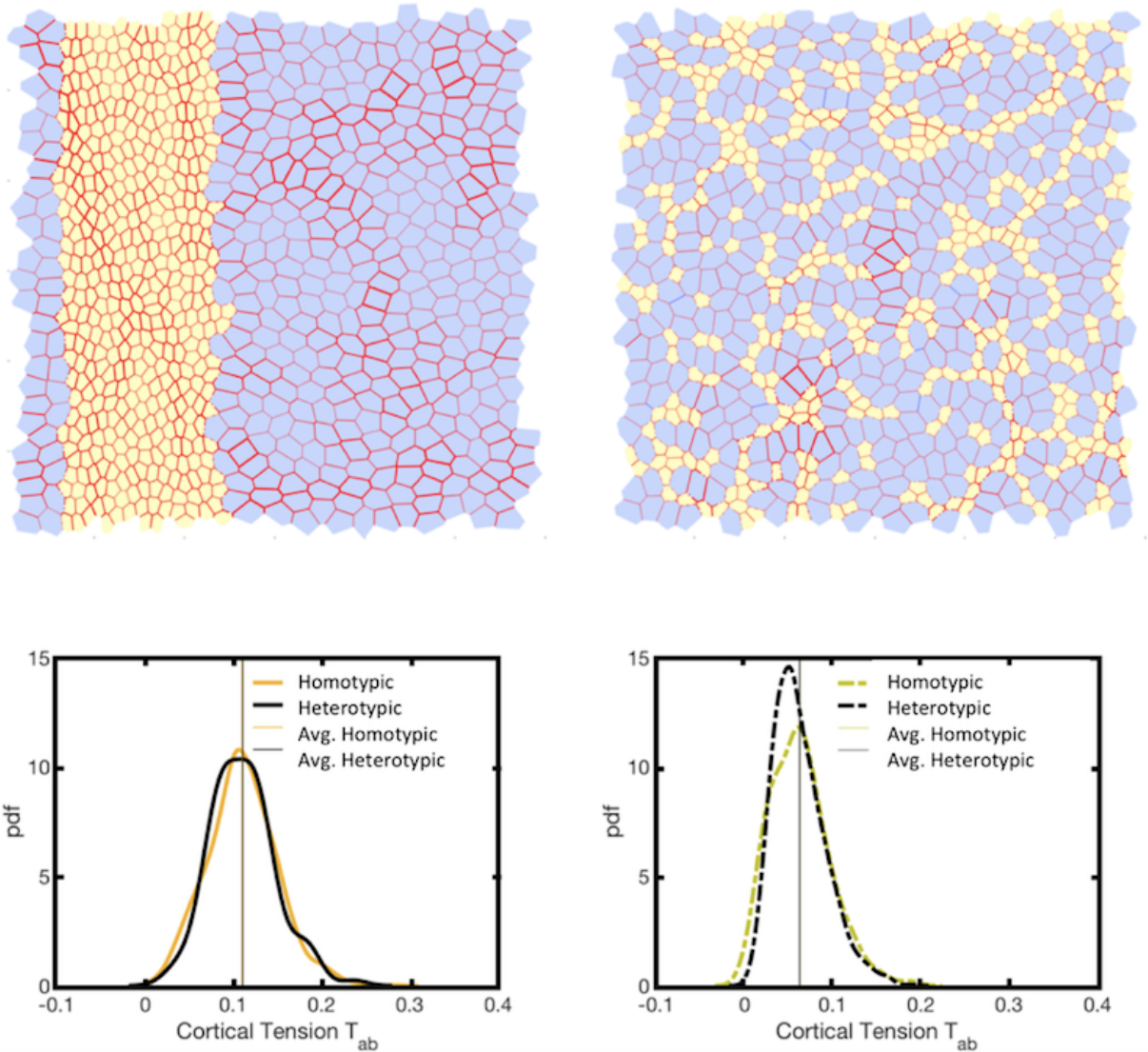


FIG. S5. *Cortical tension in area bidisperse mixtures of  $\alpha = 2.5$ .* Left and right panels shows line tension maps for sorted and mixed scenarios for a  $N = 900$  system respectively. Heterotypic edges are shown in dash-dot lines. Yellow and blue cells have  $A_0 = 0.57$  and  $1.43$  respectively. They are followed by histograms for heterotypic (in black) and homotypic (colored) edges. Vertical lines show the mean values for each curve in their respective colors.

calcium condition (Figs. S11b and c). As the demixing parameter value is rather consistent with the prediction, the pair correlation function also indicates a small-scale correlation across a couple of cell diameters. The experimental pair-correlation curve is more structureless than the predicted curve, which potentially can be understood given the variability in cell areas found for both the cell-types shown in Fig. S11c.

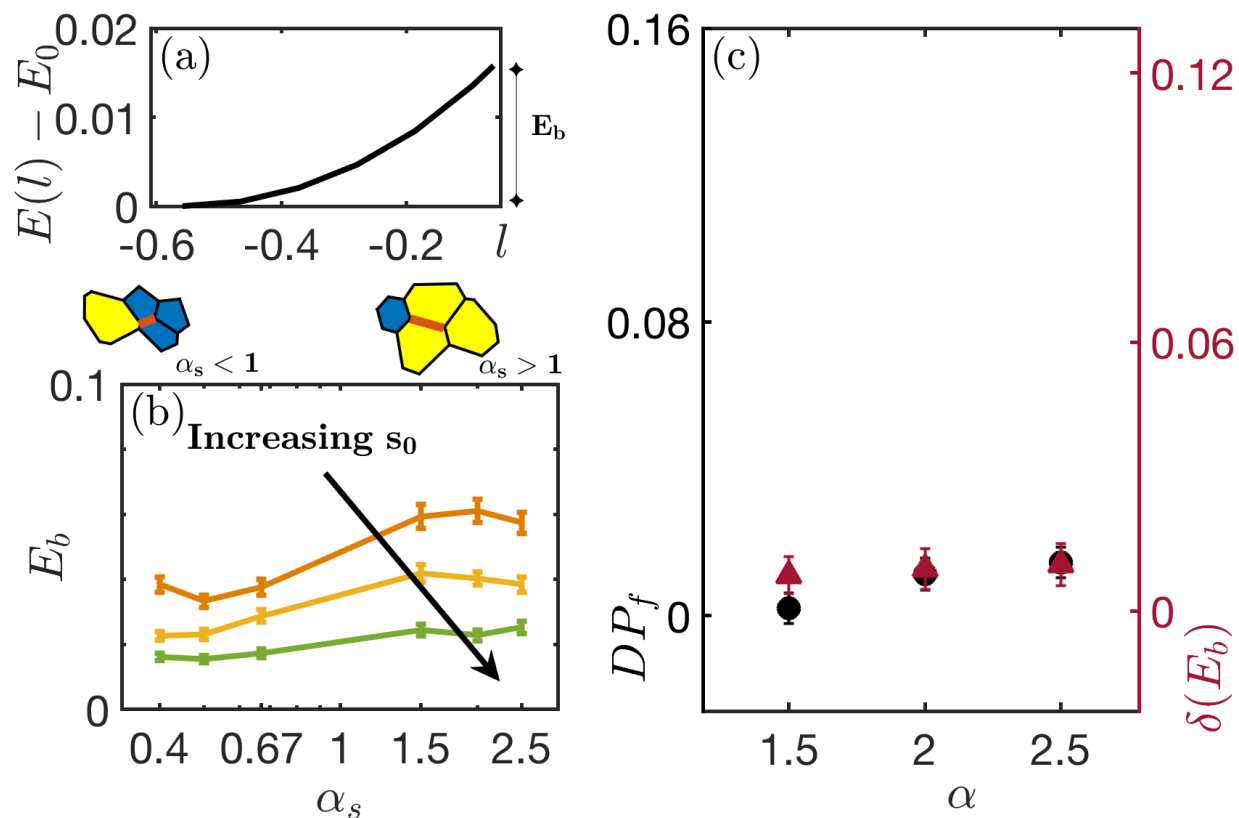


FIG. S6. *Differential energy barriers in area bidisperse mixtures.* (a) Energy  $E(l)$  relative to  $E_0$  versus T1 edglength  $l$  for a typical size bi-disperse T1 pair ( $\alpha = 2.5, s_{av} = 3.85$ ). (b) Energy Barrier  $E_b$  is plotted against area disparity  $\alpha_s$  where large values on right and small values on left imply large-cell cluster in yellow and small-cell cluster in blue respectively. Each solid curve represents the barrier for a heterotypic cell to get out of the cluster for a fixed  $s_0$  (varied from solid-like (orange) to liquid-like (green) - 3.82,3.85,3.88) (c) Correlation plot for  $s_0 = 3.85$  between Differential Energy Barriers on the right y-axis  $\delta(E_b)$  (in maroon triangles) and demixing relative to mixed scenario  $DP_f$  on the left y-axis (in black discs). Size ratio  $\alpha$  is plotted on x-axis. Simulation details provided in Table S4.

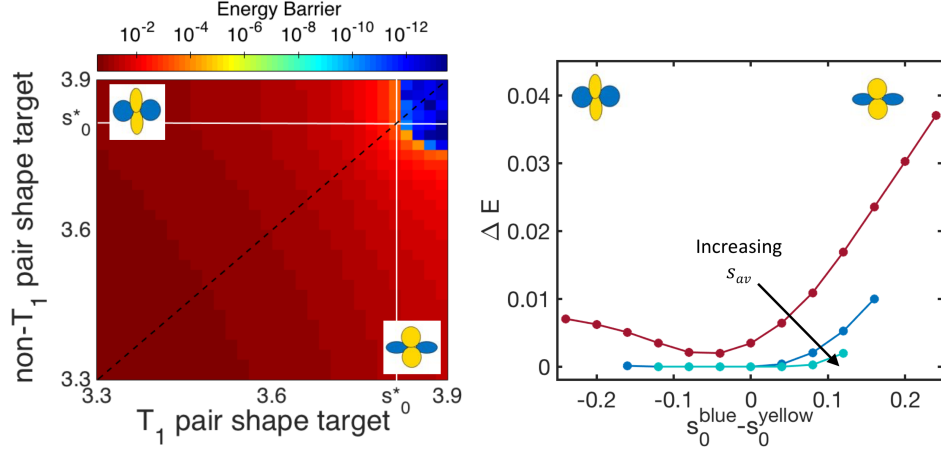


FIG. S7. *Symmetric 4-cell T1 energy barriers for shape bidispersity.* On the left is the color plot of energy barrier as a function of independently tunable shapes of T1 pair and non-T1 pair is plotted along x-axis and y-axis respectively. The dashed line represents monodisperse calculation ie for  $\Delta = 0$ . As expected it is red till it reaches the monodisperse transition point  $s_0^* = 3.813$ , after which it becomes blue. Off-diagonal phase points depict bidisperse mixtures ie  $\Delta \neq 0$ . We see that it is necessary for the T1-pair to be fluid like, for vanishing barrier. On the right is a cross-section of the phase diagram on left. Energy barrier is plotted against area disparity for increasing values of  $s_0$  3.79 to 3.85.

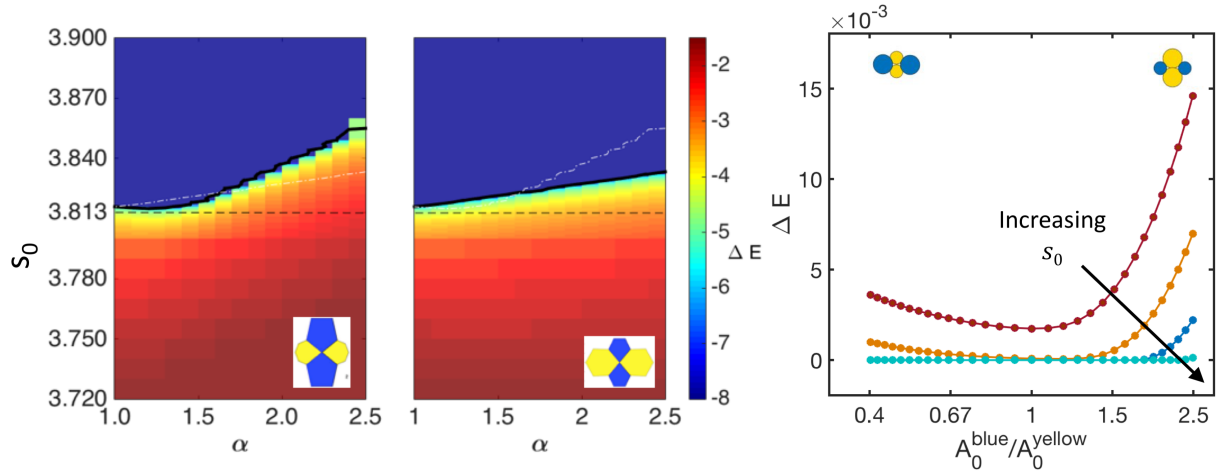


FIG. S8. *Symmetric 4-cell T1 energy barriers for area bidispersity.* On the left is the color plot of energy barrier as a function of independently tunable sizes of T1 pair (blue polygons) and non-T1 pair (yellow polygons). On the left is when blue polygons are bigger than yellow. On the right is smaller blue cells sandwiched between yellow (BssB).  $\alpha$  and  $P_0$  are the area ratios and preferred shape index respectively. Dashed black line represents the monodisperse transition point  $s_0^* = 3.813$ . This graph predicts the energy barriers to vanish at a shape index higher than  $s_0^*$  in highly bidisperse systems. On the right is a cross-section of the cumulative phase diagram on left. Energy barrier is plotted against area disparity for increasing values of  $s_0$  3.79 to 3.85.

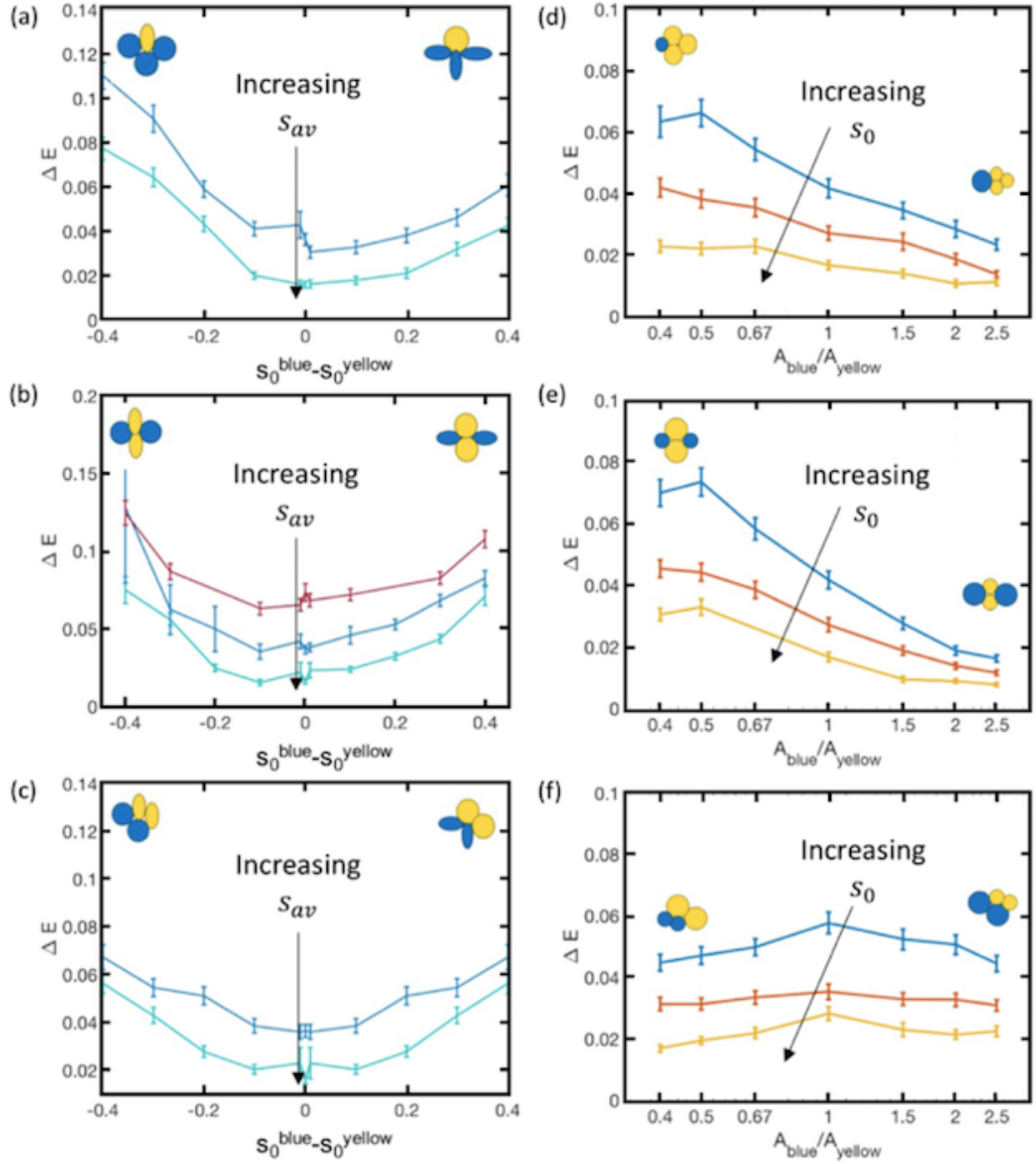


FIG. S9.  $T_1$  transitions in shape and area bidisperse mixtures. (a)-(c)  $T_1$  topologies (shown as cartoons on axis extremities) and their barrier statistics for shape bidisperse mixtures. (d)-(f)  $T_1$  topologies (shown as cartoons on axis extremities) and their barrier statistics for size bidisperse mixtures. Parameters used are in Table S4.

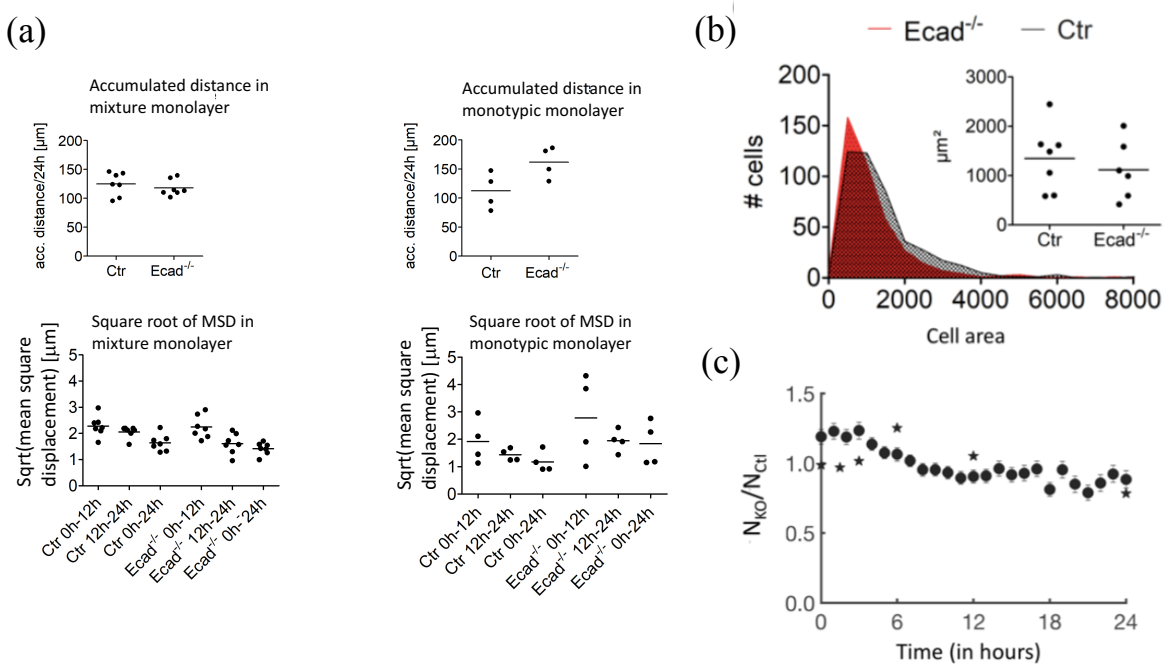


FIG. S10. *Additional quantification of cell properties.* (a) Cell displacements integrated over 24 hours in the Ctr-E-cad<sup>-/-</sup> mixtures and in the control Ctr-Ctr and E-cad<sup>-/-</sup>-E-cad<sup>-/-</sup> monotypic monolayers (cells of the same type but different tag). Ten cells from each type of the 7 Ctr-E-cad<sup>-/-</sup> demixing videos and the 4 Ctr-Ctr and Ecad<sup>-/-</sup>-Ecad<sup>-/-</sup> demixing videos are measured. We additionally show the root mean-square displacements for various time intervals for the same data sets. (b) The distribution of cell areas is shown for E-cad<sup>-/-</sup> (in red) and Ctr (in black). The inset shows the average across 6 and 7 isolates respectively, to show that area distributions are similar for both cell-types. (c) The ratio of- number of E-cad<sup>-/-</sup> (KO) to Ctr cells is plotted against time for a typical experimental co-culture. The ratio approaches unity i.e. it is almost a 50:50 mixture, over the course of the experiment.

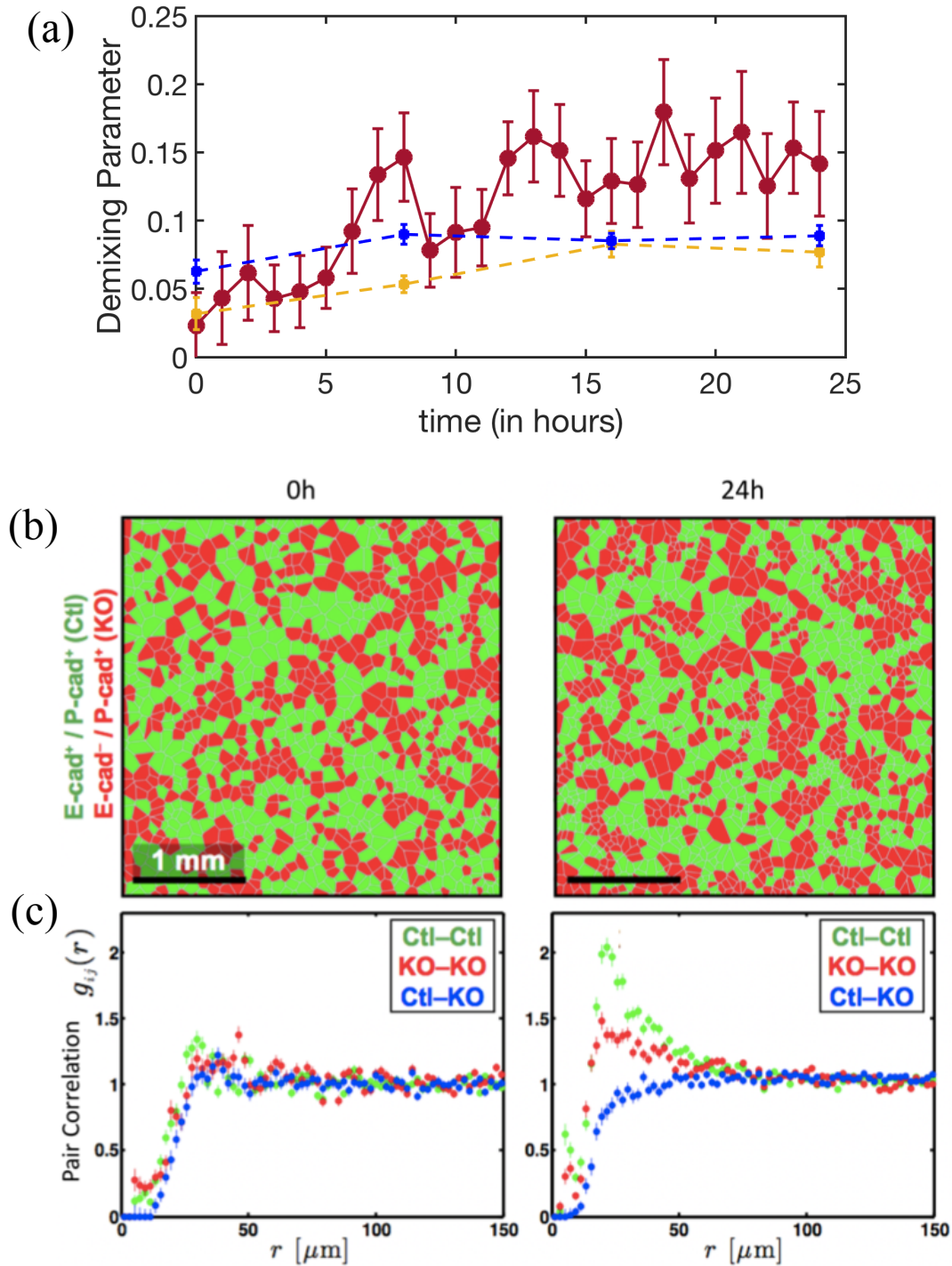


FIG. S11. *Additional quantification of experimental co-cultured monolayers.* (a) The solid maroon curve represents the time evolution of the demixing parameter for the E-cad<sup>-/-</sup> cell-type in the Ctr-E-cad<sup>-/-</sup> mixture as a function of time, averaged over 5 different monolayers using five different isolates. The maroon curve should be compared against the almost flat demixing curves for monotypic mixtures composed of 50:50 differently tagged Ctr and E-cad<sup>-/-</sup> cells shown in yellow and blue dashed curves respectively, averaged over two monolayers using two different isolates each. (b) The initial (0h) Voronoi tessellation of the co-culture nuclei, is compared side by side to the final (24h) snapshot in the high calcium condition. Green cells and red cells depict Ctr (Ctl) and E-cad<sup>-/-</sup> (KO) cells respectively. (c) The pair correlation function is plotted for the initial and final snapshots in (b). Green, red and blue markers depict correlations between- homotypic Ctl, homotypic KO, and heterotypic Ctl-KO nuclei respectively.